# SYNTHESIS OF MAGNETITE-SILICA CORE-SHELL NANOSTRUCTURES FOR PHOTODYNAMIC THERAPY

A thesis submitted in partial fulfillment of the requirement for the award of the Degree of

## Master of Science

## in

## Physics


Submitted by

**Kamaldeep Kaur**

(Roll No: 300904006)



Under the supervision of

**Dr. Bhupendrakumar Chudasama**

Assistant Professor
School of Physics and Materials Science
Thapar University
Patiala - 147004


**July 2011**

*DEDICATED TO MY LOVING PARENTS*

# *Certificate*

This is to certify that the report entitled **"Synthesis of Magnetite-silica core-shell nanostructures for photodynamic therapy"** submitted by **Ms. Kamaldeep Kaur** (Roll No. 300904006) of **M.Sc. (Physics),** Thapar University, Patiala was carried out by her under my supervision. The work presented in this thesis is her own work and is not for credit towards any other degree at Thapar University, Patiala or any other University.

13/07/2011

**(Dr. Bhupendrakumar Chudasama)**
Assistant Professor
School of Physics and Materials Science
Thapar University
Patiala - 147004

**(Dr. O. P. Pandey)**
Professor and Head
School of Physics and Materials Science
Thapar University
Patiala

**(Dr. S. K. Mohapatra)**
Dean of Academic Affairs
Thapar University
Patiala

## ACKNOWLEDGEMENT

Knowledge in itself is a continuous process. I would have never succeeded in completing my task without the cooperation, encouragement and help provided to me by various personalities. With deep sense of gratitude, I express my sincere thanks to my supervisor Dr. Bhupendra Chudasama for his keen interest, strong motivation and constant encouragement during the course of the work. I thank him for his great patience and useful suggestion apart from invaluable guidance to me.

I am grateful to Dr. O.P. Pandey, Professor and Head for his encouragement and infrastructural facilities, which he extended to me to execute this work.

I would like to convey my sincere gratitude to my friends Ms Chandani, Mr. Paramjyot Jha, Mr.Gurmeet Singh Lotey, Ms Parveer Kaur for their support, timely help and valuable discussions. I extend my sincere thanks to all the staff members of School of Physics and Materials Science for their support and encouragement.

I am also thankful to Dr. Rajesh Patel, Department of Physics, Bhavnagar University for VSM measurements.

Last but not the least; I am deeply thankful to my parents.

Above all, I render my gratitude to the Almighty God for his love and blessings.

Kamaldeep Kaur

***(Kamaldeep Kaur)***

# Abstract

Photodynamic Therapy (PDT) is a new and minimally invasive cancer treatment modality based on the photo-activation of a light-sensitive drug, photosensitiser (PS). This drug in turn generates singlet oxygen (when activated) in the malignant tissue and induces tissue necrosis or apoptosis This leads to a number of biological effects including damages to proteins, nucleic acids, lipids, and other cellular components, and often resulting in cell death and possible activation of the immune system to attack the tumour. This mode of therapy is a promising modality of treatment to malignant cancer tumours.

Core-shell nanostructures have emerged as an important class of functional materials with potential applications in diverse fields, especially in health sciences. Magnetic nanostructures have potential applications in many biological and medical fields such as drug delivery, hyperthermia treatment, magnetic resonance contrast enhancement and cell separation. In the present work, we report here synthesis and properties of a unique drug delivery system, which could be used for diagnostic and therapy purposes. Magnetite nanoparticles were synthesized by traditional coprecipitation route. These single domain magnetic nanoparticles were loaded into the surface modifiable shell of silica. Photosensitizer drug methylene blue was co-loaded into the silica shell by demethylation reaction. Hydrolysis and condensation kinetics have been established to control the shell size.

Fabricated drug delivery system was characterized by XRD, FTIR, TEM, SEM, UV-visible spectroscopy and VSM measurements. X-ray study confirms the formation of single phase magnetite nanoparticles with average size of 13.2 nm. Formation of silica shell was confirmed from the FTIR spectroscopy. Physical size of the magnetite core is 14.4 nm, which was determined through TEM measurements. This is in good agreement with the X-ray analysis. TEM micrograph also reveals that the magnetite nanoparticles are polydispersity in nature. The loading of methylene blue was also confirmed from UV-visible spectra. Room temperature magnetization measurement confirms the superparamagnetic nature of nanoparticles. The saturation magnetization of nanostructures decreases as the amount of silica in the sample increases. This is due to the increasing diamagnetic contribution from the silica shell.

The designed drug delivery system can be simultaneously loaded with multiple photosensitizer drugs and may provide a platform for controlled and sustained delivery of toxins to cancer tumors with minimal size effects.

**CONTENTS** **PAGE NUMBER**

**Certificate……..iii**

**Acknowledgement……...iv**

**Abstract……...v**

**CHAPTER 1…….....1**

**INTRODUCTION**

1.1 Failure of Chemotherapy…….……...1

1.2 Drug Targeting…….……...1

1.3 Magnetic Drug Targeting…….....3

1.3.1Mechanism…….…….4

1.4 Targeting Approaches……..4

1.4.1 Passive Approach…….…….....4

1.4.2 Active Approach…….…….5

1.5 Photodynamic Therapy……..……5

**CHAPTER 2……8**

**LITERATURE REVIEW**

**CHAPTER 3..……12**

**EXPERIMENTAL TECHNIQUE**

3.1 Synthesis of nano particles……12

3.1.1 Top Down Approach…….……12

3.1.2 Bottom Up Approach…….……...12

3.2 Synthesis of $Fe_3O_4$ Magnetite nanoparticles…….....13

3.3 Synthesis of magnetite-Silica nanostructures…….....13

3.4 Synthesis of MB loaded silica encapsulated $Fe_3O_4$ nanoparticles…….……...14

3.5 Chemical kinetics of Hydrolysis and Condensation of TEOS……..….....15

3.6 Characterisation Techniques…….....16

3.6.1 X-Ray Diffraction …….……16

3.6.2 Ultraviolet–Visible Spectroscopy..……18
3.6.3 Fourier Transform Infrared Spectroscopy…….……...20
3.6.4 Scanning Electron Microscopy…..……..……..24
3.6.5 Transmission Electron Microscopy …….……27
3.6.6 Vibrating Sample Magnetometer…..…….……29

**CHAPTER 4……...31**

**RESULTS AND DISCUSSIONS**

4.1Structural and phase analysis……31
4.1 FTIR Study…….……32
4.3 UV-Visible Spectra …….……33
4.4 Morphological Study……..…….34
4.4.1 TEM analysis…….……34
4.4.2 SEM Analysis……34
4.5 Magnetic Study ……..……35
4.6 Conclusions…….……37

**REFERENCES……..39**

**LIST OF FIGURES**

**Figure 1.1** schematic illustrations showing how nanoparticles might be used to treat cancer……..2

**Figure1.2** Photodynamic Process……..6

**Figure 1.3** The production of singlet oxygen from a photosensitisers……7

**Figure 2.1** History of PDT……..9

**Figure 3.1** X-Ray Diffractometer by PANalytical X'Pert PRO with CuKα (λ = 1.5418 Å) radiation……17

**Figure 3.2 :** Bragg's Law of reflection, the diffracted x-rays exhibit constructive interference..99 when the distance between paths of two beams differs by an integer number of wavelengths (λ) ……..18

**Figure 3.3** Schematic representation of principle of UV-Vis Spectrometer……19

**Figure 3.4** The various types of vibrations in molecules……..22

**Figure 3.5** Schematic of principle of FTIR……23

**Figure 3.6** Interaction of electron with matter……..24

**Figure 3.7 :** Schematic diagram of SEM……..26

**Figure 3.8:** The layout of TEM ……..28

**Figure3.9:** Schematic of the working principle of VSM……..29

**Figure 3.10 :** VSM Set-Up……..30

**Figure4.1:** XRD patterns of uncapped and TEOS capped $Fe_3O_4$ nanoparticles……..31

**Figure 4.2:** FTIR spectra of $Fe_3O_4$ nanoparticles coated with different concentrations of TEOS……33

**Figure 4.3: :** UV-Visible spectrum of (a) MB loaded magnetite-silica nanoparticles and (b) magnetite-silica nanoparticles ……34

**Figure 4.4:** TEM micrographs of $Fe_3O_4$ nanoparticles……35

**Figure4.5:**SEM micrograph of $Fe_3O_4$-$SiO_2$ core-shell nanostructures with different concentrations of TEOS (a) 10 µL (b) 50 µL (c) 100 µL (d) 150 µL and (e)200µL……36

**Figure 4.6:** Magnetization curve ……..36

**LIST OF TABLES**

**Table 1:** Different ranges of IR region……..22

**Table 2:** Crystallite size calculated from x-ray diffraction……..32

**Table 3:** Crystallite size calculated from x-ray diffraction…..37

# Chapter 1 Introduction

## 1.1 Failure of Chemotherapy

The unhindered spread of malignant cells called cancer. Chemotherapy has been the main modality of treatment for cancer patients; however, its success rate remains low, primarily due to limited accessibility of drugs to the tumor tissue, their intolerable toxicity, development of multi-drug resistance, and the dynamic heterogeneous biology of the growing tumors. Better understanding of tumor biology in recent years and new targeted drug delivery approaches that are being explored using different nano systems and bio-conjugates provide optimism in developing successful cancer therapy. The main reason for failure of chemotherapy is the poor accessibility of anti-neoplastic agents to the tumors, requiring higher doses, and the non-selective nature of these agents causes severe toxicity. Thus, targeted drug delivery holds immense potential to improve the treatment of cancer by selectively providing therapeutically effective drug concentrations at the tumor site [1].

## 1.2 Drug Targeting

The quest for specificity of therapeutic agents is implicit in all treatment modalities. In cancer treatment, where chemotherapeutic and radio therapeutic options are designed to kill cells, the specificity of drug action gains paramount importance. These strategies are based on the basic principle of preferentially killing cancer cells, without having any significant toxic effect on normal cells. It is necessary that all the cancer cells must be killed, either directly as a result of drug effect or indirectly due to by stander effects of the therapy in order to achieve a complete remission in patients presenting a disseminated disease. Chemotherapy regimens alone are not entirely satisfactory in aggressive carcinomas and often produce only transient responses. Combination therapy, which involves high dose of radiation with continuous infusion of chemotherapeutic agents, has been investigated for the management of un-resectable locally advanced tumors. Also, achieving therapeutically relevant drug concentrations in the tumor mass, especially in case of solid tumors for a time sufficient to allow therapeutic activity of the drug is a major problem [2]. Poor

penetrability of these drugs into the biologically heterogeneous tumor mass, leads to the residual tumor cells even after prolonged treatment with these cytotoxic agents. The high dose therapy required to maintain a state of complete remission causes intolerable systemic adverse effects, forcing the discontinuation of therapy in many patients. Most of these adverse effects impose significant compromises on the quality of life of patients. Thus, the low therapeutic indices of these treatment options have resulted in a hunt for efficient delivery systems for the available anticancer drugs, which can enable maximizing the therapeutic efficacy with minimal adverse effects.

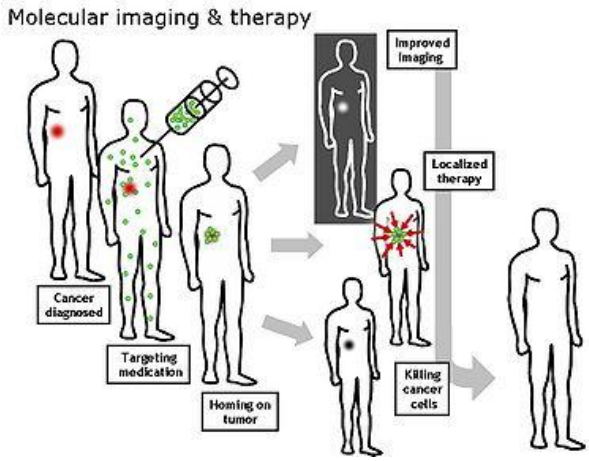


**Figure 1.1 :** Schematic illustration showing how nanoparticles might be used to treat cancer

Targeting drugs with specially designed drug delivery systems offers a lucrative option to enhance the therapeutic efficacy and to reduce the event of systemic toxicity of anti-cancer agents. The basic challenge is the transfer of drug agents to the targeted site at the appropriate time. Orally administered anticancer drugs or injections suffer from the drawback of limited control on the rate of drug release in addition to harmful side effects and toxicity. In the case of therapeutic levels extending over longer periods of time, the preferred regime is an initially high release of drug, followed by a gradual decrease with time [3].

The controlled delivery of a drug is an appropriate route to eliminate the above drawbacks and allows for continuous release of the drug. In controlled delivery, the drug delivery may commence with first-order kinetics to an optimum and effective drug concentration to the targeted region, followed by zero-order kinetics. It is possible to accomplish this by conjugating the drug to a carrier, thereby allowing the

drug to be released in a pre-designed manner. However, it is important that the carrier is biodegradable and can be eliminated by the physiological system without leaving residues that may accumulate in the cell compartments such as liposomes or tissues from the phagocytosis system. In addition, the use of carrier nanoparticles in- vivo requires them to be hydrophilic with a pH close to physiological.

### 1.3 Magnetic Drug Targeting

A number of novel drug delivery systems have emerged encompassing various routes of administration, to achieve controlled and targeted drug delivery. Magnetic field-induced, targeted drug delivery is currently attracting significant interest [4]. The conjugation of a drug to magnetic nanoparticles encapsulated with polymer is a viable method for controlled delivery of a drug to specific sites. Other potential applications of magnetic nanoparticles in biomedical and diagnostic applications include magnetic resonance imaging, hyperthermia, separation of DNA, and site-specific gene and drug delivery [5]. An important advantage of magnetic nanoparticles is the use of a localized magnetic field gradient to attract the particles to the desired site, hold them at the desired location until the therapy is completed, followed by removal. This approach necessitates that the magnetic nanoparticles have adequate magnetic strength, biocompatibility and interactive functions on the surface [6]. In this method the particles are injected intravenously and blood circulation transports these particles to the region of interest for treatment. However in this approach, it is important to consider the following aspects.

- The particles should not aggregate but rather be individually dispersed; if they are aggregated, then their spread or distribution is hindered and rapid removal from the circulation is promoted.

- When the particles are injected into the bloodstream they are rapidly coated with circulation components, such as plasma proteins. This adsorption of proteins at the particle surface is referred as opsonisation [7].

Thus, it is necessary to render the particles hydrophilic to inhibit the plasma protein coating process [8]. The targeted delivery is a viable route to increase the effective use of drug and minimize undesirable side effects and toxicity [9].

### 1.3.1 Mechanism

Magnetic drug delivery by particulate carriers is a very efficient method of delivering a drug to localized disease site. Magnetic drug transport technique is based on the fact that the drug can be either encapsulated into a magnetic microsphere (or nanosphere) or conjugated on the surface of the micro/nanosphere. When the magnetic carrier is intravenously administered, the accumulation takes place within area to which the magnetic field is applied & often augmented by magnetic agglomeration. The accumulation of the carrier at the target site allows them to deliver the drug locally. Efficiency of accumulation of magnetic carrier on diseased site depends on physiological parameters e.g. particle size, surface characteristic, field strength and blood flow rate etc. The magnetic field helps to extravasate the magnetic carrier into the targeted area. It is possible to achieve very high concentration of chemotherapeutic agents near the target site without any significant toxic effect to normal (surrounding) tissues.

Following are the major advantages of magnetic drug targeting[10]

(i) Ability to target specific locations in the body
(ii) Reduction of the quantity of drug required to attain a particular concentration in the vicinity of the target
(iii) Reduction of the concentration of the drug at non target sites

## 1.4 Targeting Approaches

### 1.4.1. Passive Approach

Passive targeting is generally making use of the anatomical and functional differences between the normal and the tumor vasculature to allow a selective accumulation of drugs at the tumor site [11]. Passive targeting occurs as a result of extravasation of the nanoparticles at the diseased site (tumor) where the microvasculature is hyper permeable and leaky, a process aided by tumor-limited lymphatic drainage. These factors lead to the selective accumulation of nanoparticles in tumor tissue, a phenomenon known as enhanced permeability and retention (EPR) [12]. The majority of solid tumors exhibit a vascular pore cut-off size between 380 nm and 780 nm, although vasculature organization may differ depending on the tumor type, its growth rate and microenvironment [13]. The use of conventional nanoparticles for drug

delivery by passive targeting would be limited to tumours in mononuclear phagocyte system organs (liver, spleen, and bone-marrow).

### 1.4.2. Active Approach

Active targeting is based on the over or exclusive expression of different epitopes or receptors in tumoral cells [14]. Thus, vectors sensitive to physical stimuli (e.g. temperature, pH, electric charge, light, sound, magnetism) have been developed and conjugated to drugs. Alternatively, active targeting may be based on over-expressed species such as low molecular weight ligands (folic acid, thiamine, and sugars), peptides (RGD, LHRD), proteins (transferrin, antibodies, lectins), polysaccharides (hyaluronic acid), polyunsaturated fatty acids, peptides, DNA, etc.

## 1.5 Photodynamic Therapy

Photodynamic therapy (PDT) is a non-invasive medicinal modality for the treatment of cancers. The therapy can be applicable to both neoplastic and non-neoplastic disease. PDT is based on the concept that certain therapeutic molecules called photosensitizers (PS) can be preferentially localized in malignant tissues, and when these PSs are activated with appropriate wavelength of light, they pass on their excess energy to surrounding molecular oxygen. This results into the generation of reactive oxygen species (ROS), such as free radicals and singlet oxygen ($^1O_2$), which are toxic to cells and tissues. This leads to a number of biological effects including damages to proteins, nucleic acids, lipids, and other cellular components, and often resulting in cell death and possible activation of the immune system to attack the tumor.

Its advantage lies in the inherent dual selectivity. First, selectivity is achieved by a preferential localization of PS in the target tissue, and second, the photo-irradiation and subsequent photodynamic action can be limited to a specific area of interest. Because the PS is nontoxic without light exposure, only the irradiated areas will be affected, even if the PS does infiltrate normal tissues.

### Photodynamic Therapy: The Process

Photodynamic therapy (PDT) is a light-activated chemotherapy in which light is used to activate a photosensitive drug that has accumulated within cells such that it causes

oxidative injury to the cells. Unlike traditional chemotherapy, which has a systemic effect, PDT achieves a localized effect. In this sense, PDT is more like a surgical or radiation therapy technique than a chemo-therapeutic treatment. The basic ingredients for a successful PDT treatment are:

(1) Drug,

(2) Light, and

(3) Oxygen

The process of photodynamic therapy begins with the photo excitation of the photosensitiser (PS) drug that has been administered to the target tissue. The photochemical process that takes place during this irradiation process lead to the production of singlet oxygen, which ultimately does the cancer cell damage.

As shown in Figure1.2, the photosensitive drug is activated by absorbing a photon to achieve its activated state. The activated drug then reacts with molecular oxygen dissolved in the cellular interior to create radical oxidizing species, usually singlet oxygen. The oxidizing radical then attacks structures of the cell via an oxidation mechanism to cause injury. Such injury may lead to cell death via coagulative necrosis or via apoptosis, depending on the choice of photosensitizing drug and the amount of drug and light administered.

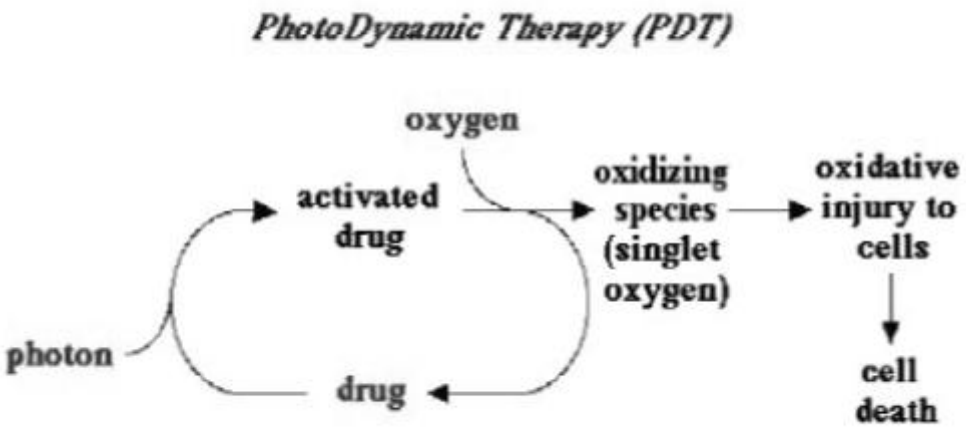


**Figure 1. 2 :** Photodynamic Process

The production of singlet oxygen is shown in figure1.3.The excited drug can then pass its energy to oxygen to create a chemical radical called “singlet oxygen.” Singlet oxygen attacks cellular structures by oxidation. Such oxidative damage might be oxidation of cell membranes or proteins. When the accumulation of oxidative damage exceeds a threshold level, the cell begins to die

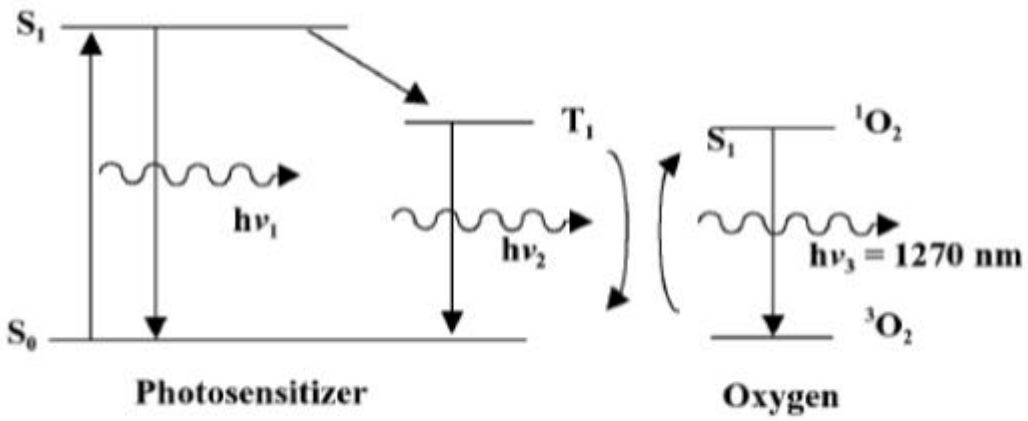


**Figure 1.3 :**The production of singlet oxygen from a photosensitiser

In the present study,we have designed a magnetic drug delivery system which is based on the concept of photodynamic therapy.

# Chapter 2 Literature Review

The history of magnetism dates back to earlier than 600 B.C., but it is only in the twentieth century that scientists have begun to understand it, and develop technologies based on this understanding. Magnetism was most probably first observed in a form of the mineral magnetite called lodestone, which consists of iron oxide a chemical compound of iron and oxygen. The ancient Greeks were the first known to have used this mineral, which they called a magnet (from Greek "Magnesian stone" ) because of its ability to attract other pieces of the same material and iron. Curiously, the first systematic study of magnetism using scientific methods was made not by a physicist but by a physician William Gilbert (1540–1603) the most distinguished man of science in England. One of the most promising fields of research lying on the border of medicine, biology, physics, chemistry, and engineering – "nanomedicine", according to the definition given by USA National Institutes of Health is based on the applications of nanotechnology for treatment, diagnosis, monitoring, and control of biological systems. In the forefront of this field is research into the rational delivery and targeting of pharmaceutical, therapeutic, and diagnostic agents. The oldest and still most vivid subfield is applications of magnetic nanoparticles (MNs) in biology and medicine. Multifunctional MNs which are the topic of this literature review have diverse potential applications in many biological and medical applications such as cell separation, drug targeting, electromagnetic hyperthermia, magnetic resonance contrast enhancement [15].

**History of photodynamic therapy**

The therapeutic use of light, as we know it, begins in 1900 when Raab reported that combination of acridine orange and light could destroy living organisms (paramecium) [16]. In the 1920s Policard [17] noted that tumor tissue was inherently more fluorescent that healthy tissue. In the 1950s Ronchese [18] attempted to achieve endogenous fluorescent molecules in tumor tissue to delineate its boundaries more accurately. Between 1940 and 1960 Figge et al. [19] and Rasmussen-Taxdal et al. [20] administered natural porphyrins to patients and tumor-bearing animals in an attempt to more accurately detect tumor tissue by fluorescence. During the 1960s Winkelman [21] used synthetic porphyrins to detect tumor tissue. Throughout the 20$^{th}$ century a few attempts were made to treat tumor tissue with photosensitizing agents, mainly

with non-porphyrin photosensitizers. Tappeiner et al. and Jesionek et al. used sunlight to achieve cosin in tumor tissue *in-vivo*. Lipson [22] had isolated a tumour localizing impurity from hematoporphyrin preparations that was later named hematoporphyrin derivative (HpD). Lipson was investigation how to detect tumor tissue by observing the intratumoral fluorescence of hematoporphyrin. He used it as a tumor detection agent [22], and recognized that it could be used as a photosensitizer to destroy tumor tissue [23]. In the 1970s Dougherty rediscovered that fluorescein diacetate could photodynamically destroy TA-3 cells in vitro [24]. In addition photodynamic therapy (PDT) has been used against bladder cancer, breast metastases, skin cancer, gynaecological, malignancies, colorectal cancers, thoractic malignancies, oral, head and neck cancer [25].

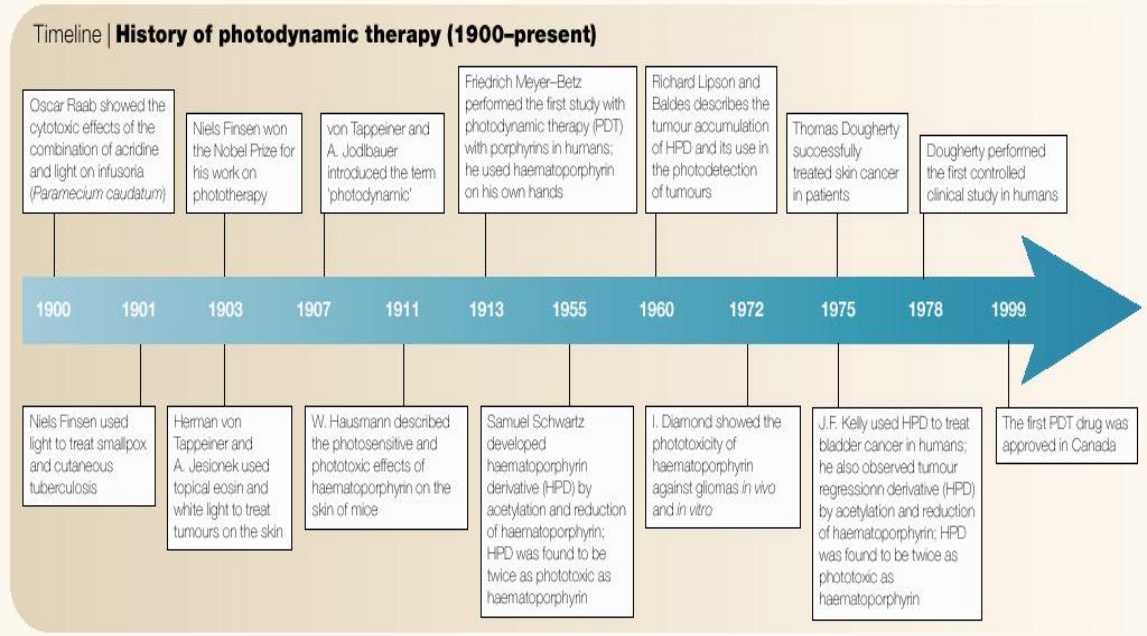


**Figure 2.1:** History of PDT (adopted from Dolmans et al. [26])

**He** et al. [27] has prepared superparamagnetic $Fe_3O_4$ nanocrystals by a chemical co-precipitation method with a thin adjustable silica layer coated on the surface by hydrolysis and condensation of tetraethyl orthosilicate. The silica-coated $Fe_3O_4$ nanocrystals were well dispersed and consisted of a 6–7 nm diameter magnetic core and silica shell about 2 nm thick. The synthesized nanocrystals have a cubic spinel structure. Their magnetic properties were carefully investigated by a SQUID magnetometer. The results showed that the nanocrystals were superparamagnetic and the blocking temperature $T_B$ shifted from 131 K down to 92 K after they were coated

with a thin nonmagnetic layer, since this layer can effectively suppress the magnetic dipolar interaction between particles; the chemically inert silica layer can limit the outside environment effect on the $Fe_3O_4$ cores quite well due to the excellent magnetic reproducibility of the coated nanocrystals after ageing for 7 months at room temperature.

**Xie** et al. [28] reports a novel way of synthesizing and functionalizing ultra-small $Fe_3O_4$ Nanoparticles as contrast agents for potential *in-vivo* tumor detection using MRI. The $Fe_3O_4$ Nanoparticles are synthesized by thermal decomposition of $Fe(CO)_5$ in the presence of 4-methylcatechol followed by oxidation. The c(RGDyK)-MC- $Fe_3O_4$ NPs show the desired biocompatibility and specificity to U87MG tumor cells. Compared to the free RGD peptide, the c(RGDyk)-MC- $Fe_3O_4$ NPs with desired size could dramatically increase the cellular uptake due to the multivalent binding. This new Nanoparticle functionalization strategy can be readily extended to couple other bioactive molecules with amine functional group to $Fe_3O_4$ Nanoparticles.

**Tada** et al. [29] present the preparation and characterization of methylene blue-containing silica-coated magnetic particles. The entrapment of methylene blue (MB) in the silica matrix took place during the growth of a silica layer over a magnetic core composed of magnetite nanoparticles. The immobilized drug can generate singlet oxygen, which was detected by its characteristic phosphorescence decay curve in the near-infrared and by a chemical method using 1,3-diphenylisobenzofuran to trap singlet oxygen. The lifetime of singlet oxygen was determined to be 52 μs (in acetonitrile) and 3 μs (in water). The release of singlet oxygen was affected by the encapsulation of MB in the silica matrix, which caused a reduction to 6% of the quantum yield of MB free in solution. The magnetization curve confirmed the superparamagnetic behaviour with a reduced saturation magnetization in respect to uncoated magnetic nanoparticles, which is consistent with the presence of a diamagnetic component over the magnetite surface. The result is a single particle platform that combines therapy (photosensitizer) and diagnostic (MRI contrast agent) possibilities at the same time, as well as drug targeting.

**Barick** et al. [30] reports the assembly of superparamagnetic $Fe_3O_4$ nanoparticles on submicroscopic $SiO_2$ spheres have been prepared by an in situ reaction using different molar ratios of $Fe^{3+/}Fe^{2+}$ (50–200%). It has been observed that

morphology of the assembly and properties of these hybrid materials composed of $SiO_2$ as core and $Fe_3O_4$ nanoparticles as shell depend on the molar ratio of $Fe^{3+}/Fe^{2+}$.

**Chen** et al. [31] reports the $Fe_3O_4@SiO_2$ core–shell structure nanoparticles prepared and characterized by TEM, FTIR, XPS and XRD. Subsequently the widely used anticancer agent doxorubicin (DOX) was successfully grafted to the surface of the core–shell nanoparticles via an amide bond with the aid of a spacer arm . The DOX-loading efficiency determined by UV–vis spectrometer was 86.5%. Drug release experiments displayed a pH-dependent behavior that DOX was cleaved from the nanoparticles easily under low pH conditions in the presence of protease and that most of the conjugated doxorubicin were released within the first 12 h. The prepared DOX-grafted $Fe_3O_4@SiO_2$ core–shell structure nanoparticles showed a superparamagnetic property with a saturation magnetization value of 49.3 emu $g^{-1}$, indicating a great potential application in the treatment of cancer using magnetic targeting drug-delivery technology.

**Qing** et al. [32] presents a simple and reproducible method was developed to synthesize a novel class of $Fe_3O_4/SiO_2/dye/SiO_2$ composite nanoparticles. As promising candidates for use in bioassays, the obtained nanoparticles have an average diameter of 30 nm, and the thickness of the outer shell of silica could be tuned by changing the concentration of the silicon precursor tetraethyl orthosilicate during the synthesis. These multifunctional nanoparticles were found to be highly luminescent, photostable and superparamagnetic. The luminescence intensity of the nanoparticles was increased as the dye concentration was increased in the preparation process. The color of the luminescence was successfully tuned by incorporating different dyes into the nanoparticles. The measurements of the emission spectra indicated that relative to the dye molecules dissolved in ethanol, the emission of the dye-doped nanoparticles exhibited either a red shift or a blue shift.

**Thomas** et al. [33] reports composite $Fe_3O_4$–$SiO_2$ materials prepared by the sol–gel method with tetraethoxysilane and aqueous-based $Fe_3O_4$ ferrofluids as precursors. The monoliths obtained were crack free and showed both optical and magnetic properties. $Fe_3O_4$ particles of 20 nm size lie within the pores of the matrix without any strong Si–O–Fe bonding. The well-established silica network provides effective confinement to these nanoparticles. The composites were transparent in the 600–800 nm regime and the field dependent magnetization curves suggest that the composite exhibits superparamagnetic characteristics.

# Chapter 3 Experimental Technique

## 3.1 Synthesis of nano materials

The nano materials can be prepared by different method categorized viz. Bottom up and Top down approaches:

### 3.1.1 Top down approach

A top-down approach is essentially the breaking down of a system into its compositional sub-systems. This involves division of a massive solid into smaller portions. This approach may involve milling or attrition, chemical methods, and volatilization of a solid followed by condensation of the volatilized components. Examples of top-down approaches are

1. High energy milling
2. Chemical mechanical milling
3. Vapour phase condensation
4. Electro-explosion
5. Laser ablation
6. Sputtering

### 3.1.2 Bottom up approach

A bottom-up approach refers to the build-up of a material from the bottom i.e. atom by atom, molecule by molecule, or cluster by cluster. In crystal growth such as atoms, ions and molecules, after impinging onto the growth surface, assemble into crystal structure one after another. The bottom –up approach plays an important role in the fabrication and processing of nanostructure and nanomaterials. There are several reasons behind this. When structures fall into a nano-scale, there is little choice for top-down approach. Bottom up approach also promises better chance to obtain nanostructures with less defects, more homogeneous chemical composition and better short and long range ordering. Bottom-up approach is driven mainly by the reduction of Gibbs free energy, so that nanostructures produced by bottom up methods are in a state closer to a thermodynamic equilibrium. On the contrary, top-down approach most likely introduces internal stress, in addition to surface defects and

contaminations. Nanolithography or nano-manipulation is a commonly used bottom-up approach. Examples of bottom-up approaches are

1. Solution combustion method
2. Sol-gel
3. Micro-emulsion
4. Reverse micelle
5. Chemical Co-precipitation, etc.

### 3.2 Synthesis of $Fe_3O_4$ magnetite nanoparticles

Magnetite ($Fe_3O_4$) nanoparticles had been synthesized by co-precipitation technique as reported earlier in literature. In a typical synthesis, stoichiometric aqueous mixture of ferric (5 mM) and ferrous (2.5 mM) ions were prepared by using ferric chloride ($FeCl_3.6H_2O$) and ferrous sulphate ($FeSO_4.7H_2O$). In these solutions 20 mM aqueous solution of ammonium hydroxide was added drop-wise under continuous stirring. Black precipitates were formed immediately. The pH of the solution was maintained at 10.5 using excess ammonia solution 25%. After continuous stirring for 20 min at room temperature (300 K), the black precipitates were magnetically decanted and washed several times with warm distilled water. The chemical reaction take place during synthesis is given below:

$$FeSO_4.7H_2O + 2FeCl_3.7H_2O + 8NH_4OH \longrightarrow Fe_3O_4 + 6NH_3Cl + (NH_4)_2SO_4 + 17H_2O$$

### 3.3 Synthesis of magnetite - silica nanostructures

In general, there are four methods use for the preparation of magnetic-silica core-shell nanostructures.

The first method is based on in-situ formation of magnetic nanoparticles inside the pores of pre-synthesized silica using metal compounds [34]. The second one involves aerosol pyrolysis. In this method precursor mixture of silicon alkoxides and metal compounds are agitated in alcohol medium followed by the decomposition of metal compounds in a flame environment [35-36]. Microemulsion is the third technique, in which non-ionic surfactants are used to form water/oil inverse microemulsion for the preparation of magnetic nanoparticles and silica layers are formed around the magnetic particles by hydrolysis and condensation of TEOS [37-39]. Fourth method is

the sol-gel technique. In this method, silica layers are formed on magnetic nanoparticles using silicon alkoxides in a basic alcohol mixture [39].

In the present study, silica coating on the pre-synthesized magnetite nanoparticles was achieved by modified hydrolysis and condensation of TEOS [41]. For this ethanol-water mixture (300 mL) was prepared by diluting 240 mL absolute ethanol with 60mL distilled water. Pre-synthesized magnetite nanoparticles were ultrasonically dispersed in 50 mL ethanol-water. Different concentration of TEOS (10, 50, 100, 150, 200 μL) was added drop-wise into the ethanol-water mixture. Upon addition, the hydrolysis and condensation of TEOS begins immediately, which nucleates silica nanoparticles into the reaction mixture. After 20 min of commencement of hydrolysis and condensation, solution of ethanol-water mixture containing magnetite nanoparticles was added drop-wise into the beaker.

Presence of pre-synthesized silica nanoparticles suppresses magnetic dipolar interaction and prevents the agglomeration of magnetite nanoparticles [42]. The solution was stirred at room temperature (300 K) for 10 h. During this time, a fine layer of silica is formed over magnetite nanoparticles. pH of the reaction was maintained at 12 during the entire reaction period, this growth secondary silica particles encapsulates finely coated magnetite nanoparticles and produced silica encapsulated magnetite nanostructures.

Silica encapsulated magnetite nanostructure were isolated by magnetic decantation. Unreacted TEOS (if any), and surface impurities were removed from the nanostructures by washing them with absolute ethanol. These samples were vacuum dried at room temperature.

### 3.4 Synthesis of Methylene Blue (MB) loaded silica encapsulated $Fe_3O_4$ nanostructures

Pre-synthesized $Fe_3O_4$ nanoparticles coated with silica were dispersed in a mixture, containing 5 mg of Methylene Blue **(**MB) was added and pH was again adjusted to 12 with the help of $NH_4OH$. MB loaded $Fe_3O_4$-$SiO_2$ core-shell nanostructures have been isolated from the solution by magnetic decantation. This DDV were washed with

absolute ethanol until traces of MB were observed in Uv-visible spectrum of the supernatant.

### 3.5 Chemical kinetics of hydrolysis and condensation of TEOS

Magnetite-silica core-shell nanospheres have been produced by adopting a two-step process. In the first step, pre-synthesized magnetite nanoparticles were delicately coated with a thin layer of silica. The addition of TEOS in the mixture of ethanol-water begins the hydrolysis and condensation of TEOS. First, TEOS hydrolyzed into silicic acid [43],

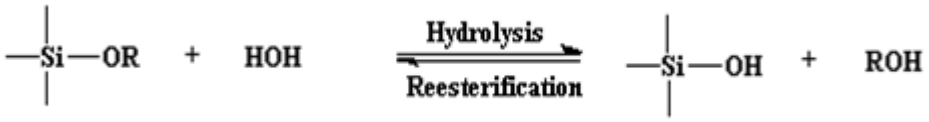


where R is an alkyl group. Hydrolysis of alkoxysilanes occurred by nucleophilic mechanism. Under the basic condition, water dissociates to produce nucleophilic hydroxyl anions ($OH^-$), and then the hydroxyl anion attacks the silicon atom. When an alkoxide group (OR) is replaced by a hydroxyl group (OH), the electron density of silicon is reduced, accelerating the hydrolysis rate of other alkoxides. Once an alkoxide group is hydrolyzed, the others would hydrolyze rapidly [43].

Next, the silicic acid condenses into primary silica particles either by water or alcohol condensation mechanism [41].

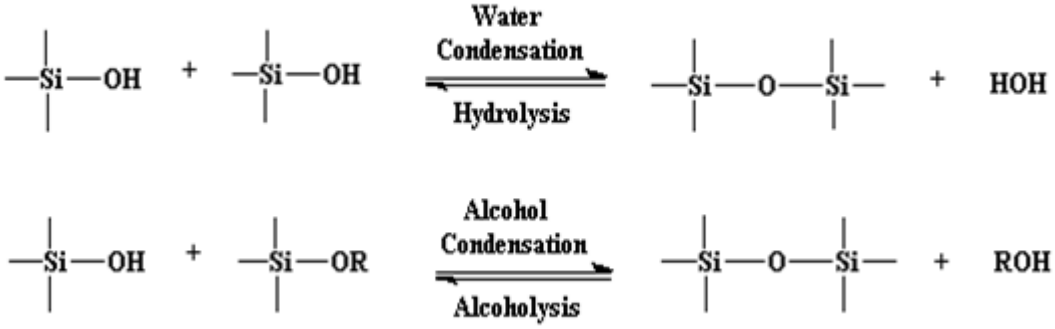


Alkoxide groups produced by the hydrolysis are polymerized into $SiO_2$ by the formation of siloxane bonds through water or alcohol condensation. The condensation of $Si(OH)_4$ will nucleate embryos of silica.

These embryos are colloidally unstable and readily aggregate into larger particles with surface charge large enough to prevent the irreversible Brownian aggregation. These silica nanoparticles will chemically adsorbed on the surface of magnetite nanoparticles by the formation of covalent bond between Fe of magnetite and $OH^-$ ions on the surface of silica [37-44].

In the second step, by keeping the growth conditions intact, the hydrolyzed silica embryos diffuse rapidly and produce cages of silica with a well-defined morphology in which, lightly coated magnetite nanoparticles were entrapped. The strong pH environment leads to the isotropic growth [45] which, results into the formation of, nanospheres of silica encapsulated magnetic nanoparticles. Two-step process is necessary to preserve the monodomain nature of magnetic nanoparticles [46].

### 3.6 Characterisation Techniques

The characterization of materials regarding determination of elemental composition, estimation of trace impurities, structural analysis, morphological analysis, magnetic analysis, identification of crystalline phases and information on crystal defects play an important role for the quality control and development of advanced materials and their use in precision devices. The nanostructures have been characterized for their structural, compositional, morphological, optical, magnetic and chemical properties. The techniques include X-ray diffraction (XRD), UV-visible absorption spectroscopy, Fourier transform infrared spectroscopy (FTIR), Scanning electron microscopy (SEM), Transmission electron microscopy (TEM), Vibrational Sample Magnetometer (VSM).

#### 3.6.1 X-Ray Diffraction (XRD)

X-ray diffraction (XRD) is a versatile technique that reveals detailed information about the chemical composition and crystallographic structure of natural and synthesized materials. X-Ray Diffractometer by PANalytical X'Pert PRO with CuKα (λ = 1.5418 Å) radiation operated at 45 kV and 40 mA, is shown in the figure 3.1

**Bragg's law**:

When a crystal is bombarded with X-rays of a fixed wavelength and at certain incident angles, intense reflected X-rays are produced when the wavelengths of the

scattered X-rays interfere constructively. In order for the waves to interfere constructively, the differences in the travel path must be equal to integral multiples of the wavelength. When this constructive interference occurs, a diffracted beam of X-rays will leave the crystal at an angle equal to that of the incident beam. To illustrate this feature, consider a crystal with crystal lattice planar distances d, where the travel path length difference between the ray paths of two beams is an integer multiple of the wavelength, constructive interference will occur for a combination of that specific wavelength, crystal lattice planar spacing and angle of incidence (θ). Each rational plane of atoms in a crystal will undergo refraction at a single, unique angle (for X-rays of a fixed wavelength). The general relationship between the wavelengths of the incident X-rays, angle of incidence and spacing between the crystal lattice planes of atoms is known as Bragg's Law. i.e.

$$\mathbf{2\ d\ Sin\theta = n\lambda}$$

Where n is an integer that indicates the order of diffraction, λ is the wavelength of the incident X- rays, d is the interplanar spacing of the crystal and θ is the angle of incidence.

**Figure 3.1:** X-Ray Diffractometer by PANalytical X'Pert PRO with CuKα (λ = 1.5418 Å) radiation.

X-ray diffraction is an efficient analytical technique used to identify and characterize unknown crystalline materials. Monochromatic X-rays are used to determine the interplanar spacing of the unknown materials. Samples are analysed as

powders with grains in random orientations to insure that all crystallographic directions are "sampled" by the beam. When the Bragg conditions for constructive interference are obtained, a "reflection" is produced, and the relative peak height is generally proportional to the number of grains in a preferred orientation. The geometry of an X-ray diffractometer is such that the sample rotates in the path of the collimated X-ray beam at an angle θ while the X-ray detector is mounted on an arm to collect the diffracted X-rays and rotates at an angle of 2θ. The instrument used to maintain the angle and to rotate the sample is termed a goniometer.

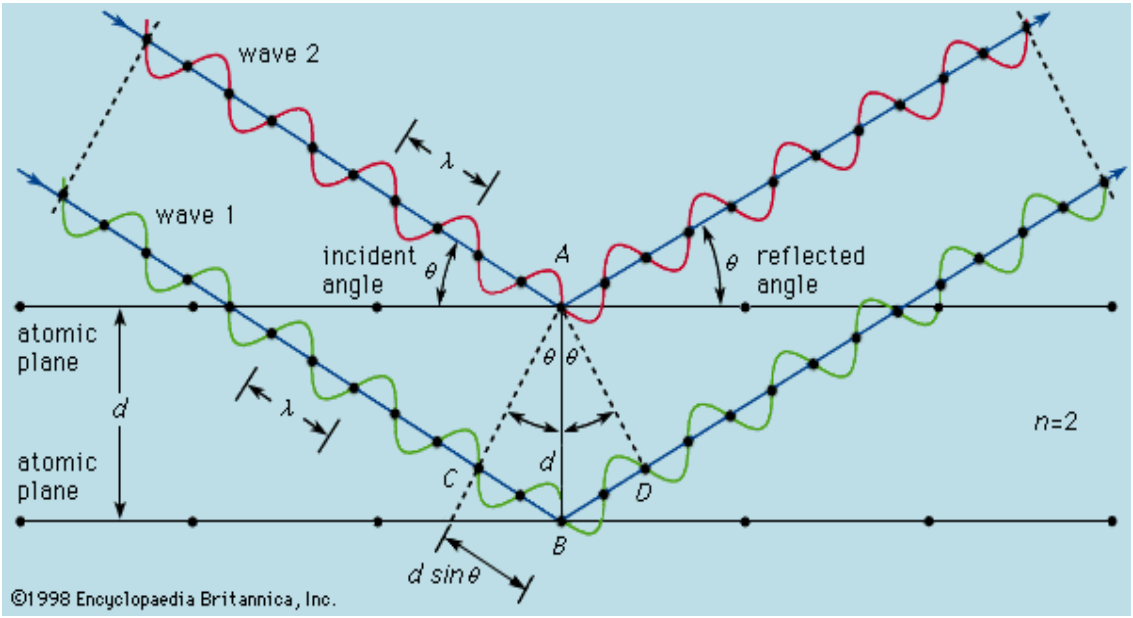


**Figure 3. 2:** Bragg's Law of reflection, the diffracted x-rays exhibit constructive interference when the distance between paths of two beams differs by an integer number of wavelengths (λ)

**X-ray diffraction can be used to determine**

- Degree of crystallinity
- Crystalline phase, and crystal structure
- Crystallite size from analysis of peak broadening
- Crystallite shape from study of peak symmetry

### 3.6.2 Ultraviolet–Visible spectroscopy

The Ultraviolet-Visible (UV-Vis) Spectroscopy is an analytical technique that uses light in the visible (VIS), ultraviolet and near infrared ranges. UV-Vis spectroscopy refers to absorption spectroscopy in the ultraviolet-visible spectral region. In this

region of the electromagnetic spectrum, molecules undergo electronic transitions. This technique is complementary to fluorescence spectroscopy. The absorption of light occurs very quickly femto-second time scale. The energy in a quantum (Planck's Law) is expressed by the equation:

$$\mathbf{E = h\nu = hc/\lambda}$$

Where E is the energy, h is Planck's constant, **ν** and **λ** are the frequency and wavelength of the incoming photon, and **c** is the speed of light.

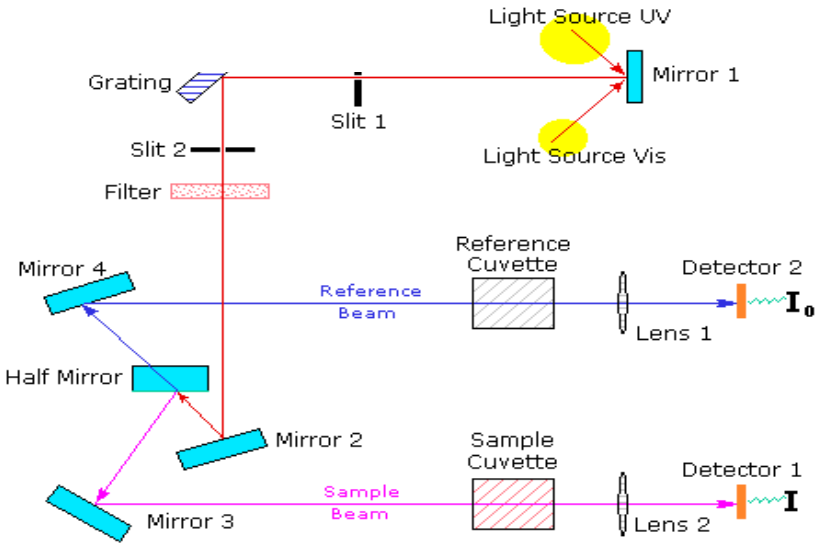


**Figure 3.3:** Schematic representation of principle of UV-Vis Spectrometer

Absorption of light by solution is one of the oldest and still one of the more useful instrumental methods. The wavelength of light that a compound will absorb is characteristic of its chemical structure. Specific regions of the electromagnetic spectrum are absorbed by exciting specific types of molecular and atomic motion to higher energy levels. Absorption of microwave radiation is generally due to excitation of molecular rotational motion. Infrared absorption is associated with vibrational motions of molecules. Absorption of visible and ultraviolet (UV) radiation is associated with excitation of electrons, in both atoms and molecules, to higher energy states. All molecules will undergo electronic excitation following absorption of light, but for most molecules very high energy radiation (in the vacuum ultraviolet, <200 nm) is required. For molecules containing conjugated electron systems however, light in the UV-visible region is adequate. As the degree of conjugation increases, the spectrum shifts to lower energy.

Principle of UV-visible spectrometer is shown in the figure 3.3. A beam of light from a visible and/or UV light source (colored red) is separated into its component wavelengths by a prism or diffraction grating. Each monochromatic beam in turn is split into two equal intensity beams by a half-mirrored device. One beam, the sample beam (colored magenta), passes through a small transparent container (cuvette) containing a solution of the compound being studied in a transparent solvent. The other beam, the reference (colored blue), passes through an identical cuvette containing only the solvent. The intensities of these light beams are then measured by electronic detectors and compared. The intensity of the reference beam, which should have suffered little or no light absorption, is defined as $I_o$. The intensity of the sample beam is defined as I. Over a short period of time, the spectrometer automatically scans all the component wavelengths in the manner described. The ultraviolet (UV) region scanned is normally from 200 to 400 nm, and the visible portion is from 400 to 800 nm. Beer-Lambert Law: The Beer-Lambert law states that the absorbance of a solution is directly proportional to the concentration of the absorbing species in the solution and the path length. Thus, for a fixed path length, UV/VIS spectroscopy can be used to determine the concentration of the absorber in a solution. It is necessary to know how quickly the absorbance changes with concentration. The amount of light, I, transmitted through a solution of an absorbing chemical in a transparent solvent can be related to its concentration by Beers Law:

$$- \log I/I_o = A = \varepsilon_\lambda bc$$

where $I_o$ is the incident light intensity, A is the absorbance, b is the cell path length in cm, c is the solution concentration in moles/litre, and $\varepsilon_\lambda$ is the molar absorptivity, (also referred to as the molar extinction coefficient), which has units of litre/mole/cm, and $\varepsilon_\lambda$ is a function of wavelength.

### 3.6.3 Fourier Transform Infrared Spectroscopy

FTIR spectroscopy is used primarily for qualitative and quantitative analysis of organic compounds, and also for determining the chemical structure of many inorganics. Fourier transform infrared spectroscopy (FTIR) is a technique which is used to obtain an infrared spectrum of absorption, emission, photoconductivity or Raman scattering of a solid, liquid or gas. FTIR spectrometer simultaneously collects spectral data in a wide

spectral range. This confers a significant advantage over a dispersive spectrometer which measures intensity over a narrow range of wavelengths at a time. FTIR technique has made dispersive infrared spectrometers all but obsolete. The term Fourier transform infrared spectroscopy originates from the fact that a Fourier transform (a mathematical algorithm) is required to convert the raw data into the actual spectrum. The main goal of IR spectroscopic analysis is to determine the chemical functional groups in the sample. Different functional groups absorb at characteristic frequencies.

At temperatures above absolute zero, all the atoms in molecules are continuous vibrates. When the frequency of a specific vibration is equal to the frequency of the IR radiation directed on the molecule, the molecule absorbs the radiation. Each atom has three degrees of freedom, corresponding to motions along any of the three Cartesian coordinate axes (x, y, z). A polyatomic molecule of *n* atoms has 3*n* total degrees of freedom. However, 3 degrees of freedom are required to describe translation, the motion of the entire molecule through space. Additionally, 3 degrees of freedom correspond to rotation of the entire molecule. Therefore, the remaining $3n - 6$ degrees of freedom are true, fundamental vibrations for nonlinear molecules. Linear molecules possess $3n - 5$ fundamental vibrational modes because only 2 degrees of freedom are sufficient to describe the rotation. Among the $3n - 6$ or $3n - 5$ fundamental vibrations (also known as normal modes of vibration), those that produce a net change in the dipole moment may result in an IR activity and those that give polarizability changes may give rise to Raman activity. Naturally, some vibrations can be both IR- and Raman-active.

The total number of observed absorption bands is generally different from the total number of fundamental vibrations. It is reduced because some modes are not IR active and a single frequency can cause more than one mode of motion to occur. Conversely, additional bands are generated by the appearance of overtones (integral multiples of the fundamental absorption frequencies), combinations of fundamental frequencies, differences of fundamental frequencies, coupling interactions of two fundamental absorption frequencies, and coupling interactions between fundamental vibrations and overtones or combination bands (Fermi resonance). The intensities of overtone, combination, and difference bands are less than those of the fundamental

bands. The combination and blending of all the factors thus create a unique IR spectrum for each compound.

The major types of molecular vibrations are stretching, bending, rocking, wagging, and twisting. The various types of vibrations are illustrated in Fig3.4. Infrared radiation is absorbed and the associated energy is converted into these types of motions. Absorption involves discrete, quantized energy levels. However, the individual vibrational motion is usually accompanied by other rotational motions. These combinations lead to the absorption bands, not the discrete lines, commonly observed in the mid IR region. The IR spectra are commonly divided into three smaller areas: near IR, mid IR, and far IR Table 1.

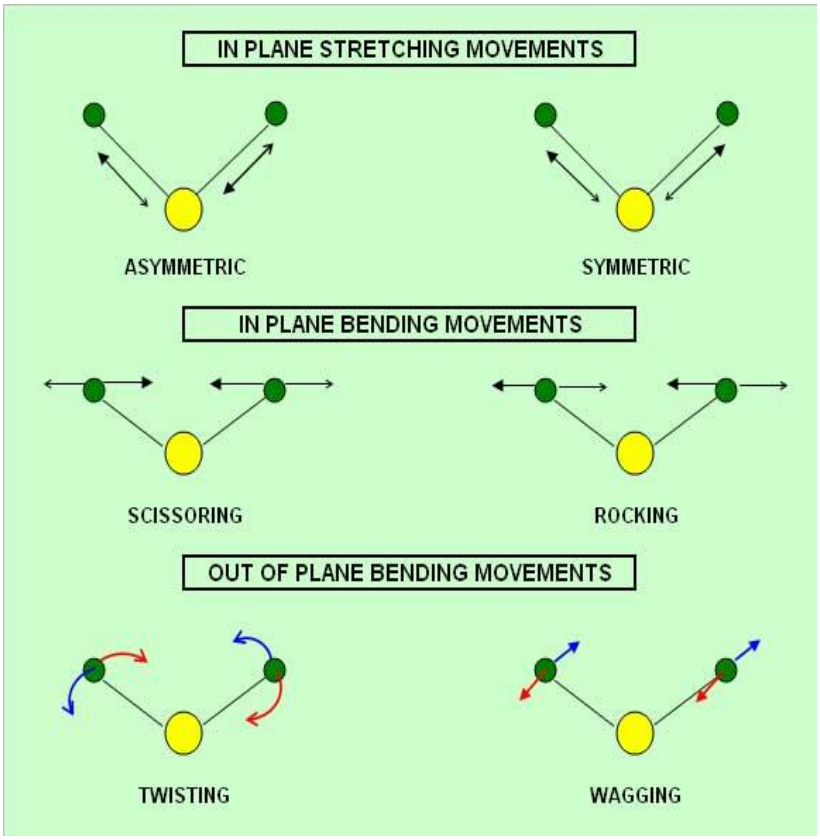


**Figure 3.4:** The various types of vibrations in molecules

| | **Near IR** | **Mid IR** | **Far IR** |
|---|---|---|---|
| **Wavenumber ($cm^{-1}$)** | 13000-4000 | 4000-200 | 200-10 |
| **Wavelength (μm)** | 0.78-2.5 | 2.5-50 | 50-1000 |

**Table 1**: Different ranges of IR region

**Principle of Operation:** Chemical bonds absorb infrared energy at specific frequencies (or wavelengths); the basic structure of compounds can be determined by the spectral locations of their IR absorptions. The plot of a compound's IR transmission vs. frequency is its "fingerprint", which when compared to reference spectra identifies the material. FTIR spectrometers offer speed and sensitivity impossible to achieve with earlier wavelength-dispersive instruments. This capability allows rapid analysis of samples down to the nano-gram level in some cases, making the FTIR unmatched as a problem-solving tool in organic chemistry.

An FT-IR is typically based on a Michelson Interferometer. The interferometer consists of a beam splitter, a fixed mirror, and a mirror that translates back and forth, very precisely. The beam splitter is made of a special material that transmits half of the radiation striking it and reflects the other half. Radiation from the source strikes the beam splitter and separates into two beams. One beam is transmitted through the beam splitter to the fixed mirror and the second is reflected off the beam splitter to the moving mirror. The fixed and moving mirrors reflect the radiation back to the beam splitter. Again, half of this reflected radiation is transmitted and half is reflected at the beam splitter**,** resulting in one beam passing to the detector and the second back to the source.

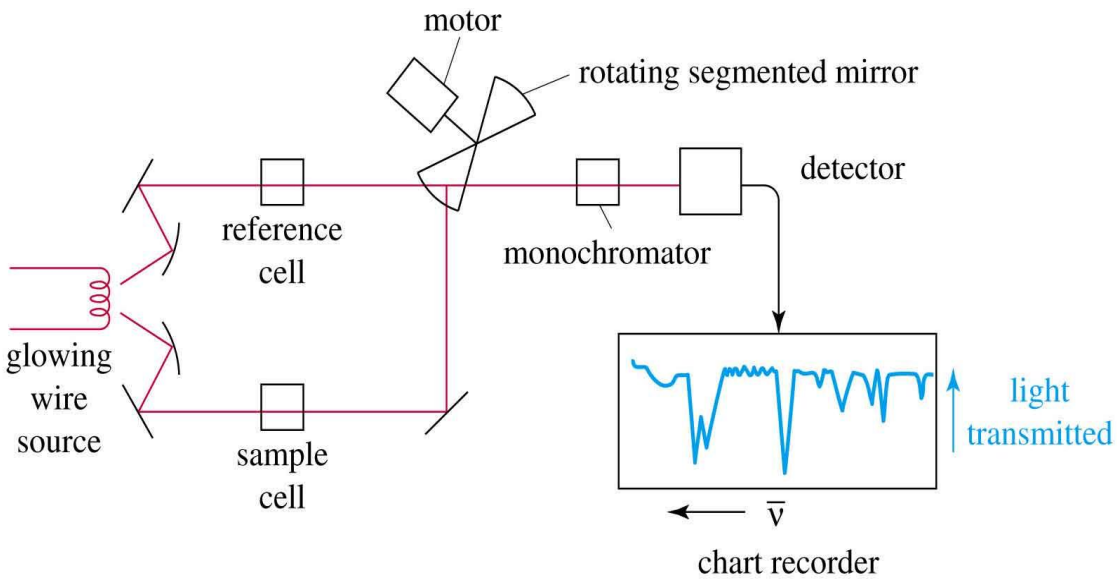


**Figure 3.5:** Schematic of principle of FTIR

**Applications of FTIR spectroscopy include:**

- Materials evaluation and identification Organic compounds
  Chemical of inorganic compounds
  Deformulations
  Forensics
  Material homogeneity
- Failure analysis
  Micro-contamination identification
  Adhesive performance
  Material delamination
  Corrosion chemistry
- Quality control screening
  "Good" to "bad" sample comparison
  Evaluation of cleaning procedure effectiveness
  Comparison of materials from different lots or vendo

### 3.6.4 Scanning Electron Microscope

Scanning electron microscope (SEM) is a type of electron microscope that images a sample by scanning it with a high-energy beam of electrons in a raster scan pattern.

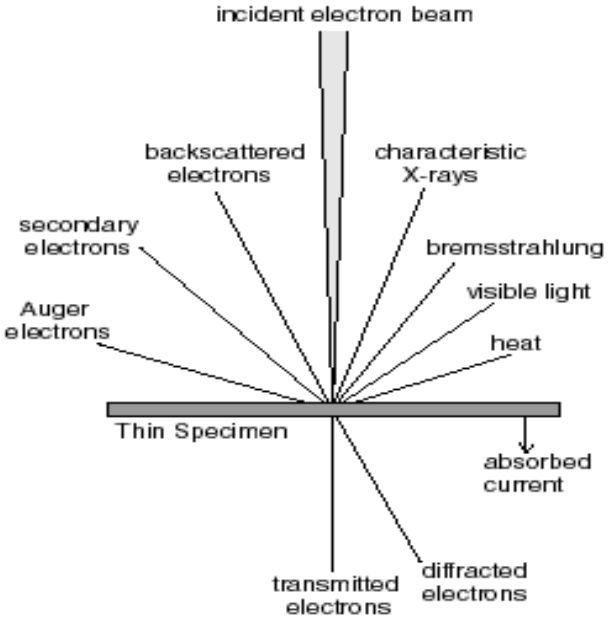


**Figure 3.6:** Interaction of electron with matter

The electrons interact with the atoms that make up the sample producing signals that contain information about the sample's surface topography, composition, and other properties such as electrical conductivity. Electron bombardment of a sample is unique to microprobe analysis and produces a large number of effects from the target material figure 3.6. The incident electrons interact with specimen atoms and are significantly scattered by them (rather than penetrating the sample in a linear fashion). Most of the energy of an electron beam will eventually end up heating the sample (phonon excitation of the atomic lattice); however, before the electrons come to rest, they undergo two types of scattering: elastic and inelastic.

In elastic scattering, the electron trajectory changes, but its kinetic energy and velocity remain essentially constant (due to large differences between the mass of the electron and nucleus). This process is known as electron backscattering (although later we will confine the term "backscattered electrons" to those scatter out of the sample).

In inelastic scattering, the trajectory of the incident electron is only slightly perturbed, but energy is lost through interactions with the orbital electrons of the atoms in the specimen. Inelastic interactions produce diverse effect including:

- phonon excitation (heating)
- cathodoluminescence (visible light fluorescence)
- continuum radiation (bremsstrahlung or “braking” radiation)
- characteristic x-rays
- plasmon production (secondary electrons)
- Auger electron production (ejection of outer shell electrons)

SEM uses a focused beam of high-energy electrons to generate variety of signals at the surface of solid specimens. The signals that derive from electron-sample interactions reveal information about the sample including external morphology (texture), chemical composition, and crystalline structure and orientation of materials making up the sample. In most applications, data are collected over a selected area of the surface of the sample, and a 2-dimensional image is generated that displays spatial variations in these properties. Areas ranging from approximately 1 cm to 5 microns in width can be imaged in a scanning mode using conventional SEM techniques

(magnification ranging from 20X to approximately 30,000X, spatial resolution of 50 to 100 nm). The SEM is also capable of performing analyses of selected point locations on the sample; this approach is especially useful in qualitatively or semi-quantitatively analysis of chemical compositions (using EDS), crystalline structure, and crystal orientations (using EBSD).

**Principles :** Accelerated electrons in an SEM carry significant amounts of kinetic energy, and this energy is dissipated as a variety of signals produced by electron-sample interactions when the incident electrons are decelerated in the solid sample. These signals include secondary electrons (that produce SEM images), backscattered electrons (BSE), diffracted backscattered electrons (EBSD that are used to determine crystal structures and orientations of minerals), photons (characteristic X-rays that are used for elemental analysis and continuum X-rays), visible light (cathodoluminescence-CL), and heat. Secondary electrons and backscattered electrons are commonly used for imaging samples: secondary electrons are most valuable for showing morphology and topography on samples and backscattered electrons are most valuable for illustrating contrasts in composition in multiphase samples (i.e. for rapid phase discrimination).

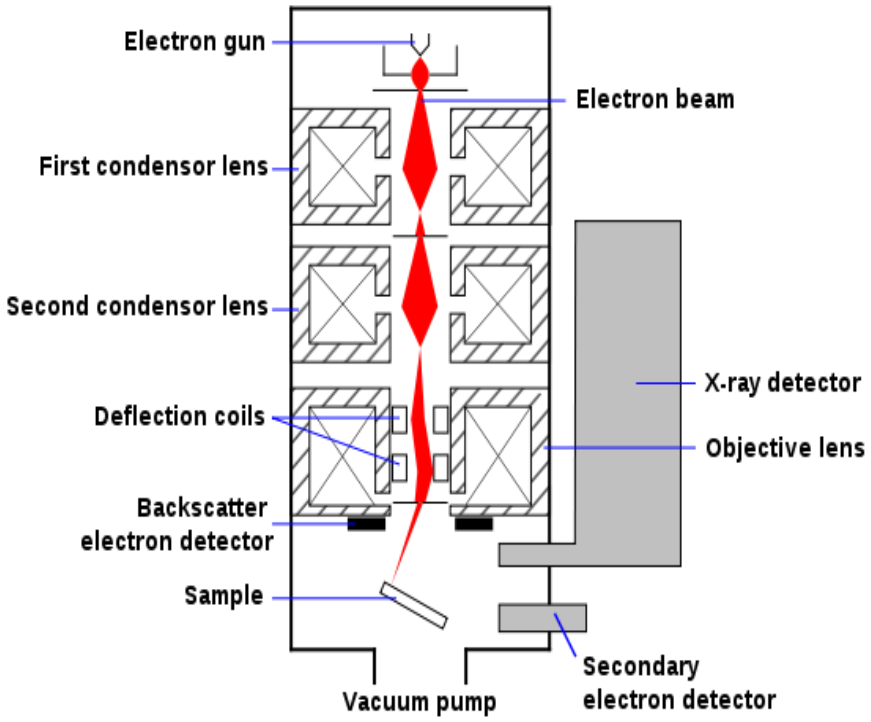


**Figure 3.7:** Schematic diagram of SEM

X-ray generation is produced by inelastic collisions of the incident electrons with electrons in discrete ortitals (shells) of atoms in the sample. As the excited electrons return to lower energy states, they yield X-rays that are of a fixed wavelength (that is related to the difference in energy levels of electrons in different shells for a given element). Thus, characteristic X-rays are produced for each element in a mineral that is "excited" by the electron beam. SEM analysis is considered to be "non-destructive"; that is, x-rays generated by electron interactions do not lead to volume loss of the sample, so it is possible to analyse the same materials repeatedly.

**Applications**

SEM is routinely used to generate high-resolution images of objects and to determine spatial variations in chemical compositions.

1) Acquiring elemental maps or spot chemical analyses using EDS,
2) Discrimination of phases based on mean atomic number (commonly related to relative density) using BSE, and
3) Compositional maps based on differences in trace element "activators" (typically transition metal and Rare Earth elements) using CL.

The SEM is also widely used to identify phases based on qualitative chemical analysis and/or crystalline structure. SEMs equipped with diffracted backscattered electron detectors (EBSD) can be used to examine micro fabric and crystallographic orientation in many materials.

### 3.6.5 Transmission electron microscopy (TEM)

Transmission electron microscopy (TEM) is a microscopy technique whereby a beam of electrons is transmitted through an ultra-thin specimen, interacting with the specimen as it passes through. An image is formed from the interaction of the electrons transmitted through the specimen; the image is magnified and focused onto an imaging device, such as a fluorescent screen, on a layer of photographic film, or to be detected by a sensor such as a CCD camera. TEMs are capable of imaging at a significantly higher resolution than light microscopes, owing to the small de Broglie wavelength of electrons. This enables the instrument's user to examine fine detail-even as small as a single column of atoms, which is tens of thousands times smaller

than the smallest resolvable object in a light microscope. TEM forms a major analysis method in a range of scientific fields, in both physical and biological sciences. At smaller magnifications TEM image contrast is due to absorption of electrons in the material, due to the thickness and composition of the material. At higher magnifications complex wave interactions modulate the intensity of the image, requiring expert analysis of observed images. Alternate modes allow TEM to observe modulations in chemical identity, crystal orientation, electronic and structure.

The TEM is composed of several components, which include a vacuum system in which the electrons travel an electron emission source for generation of the electron stream, a series of electromagnetic lenses, as well as electrostatic plates. The latter two allow the operator to guide and manipulate the beam as required.

**Applications**

The instrument allows performing the following analyses:

- Morphological analysis,
- Electronic diffraction,
- EDS qualitative and semi-quantitative analysis, either in Spot or in Semi-Stem mode.

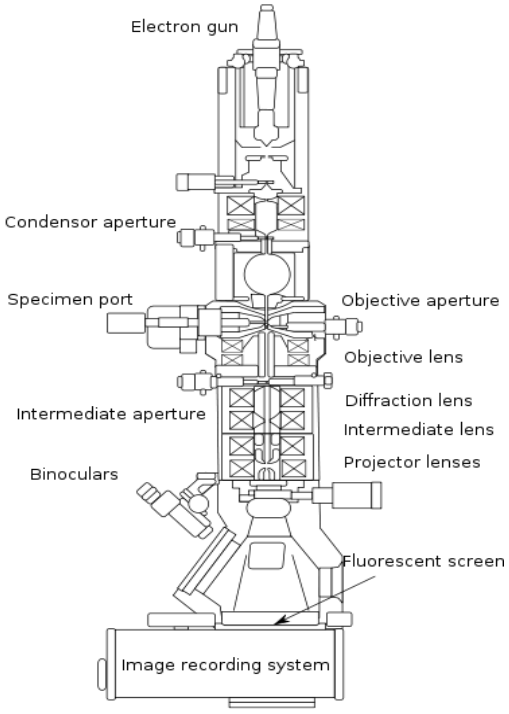


**Figure 3.8:** The layout of TEM

### 3.6.6 Vibrating Sample Magnetometer

A vibrating sample magnetometer (VSM) is a scientific instrument that is used relatively widespread for magnetic measurements.

**Principle:** If a sample of any material is placed in a uniform magnetic field, created between the poles of an electromagnet, a dipole moment will be induced. If the sample vibrates with sinusoidal motion a sinusoidal electrical signal can be induced in suitable placed pick-up coils. The signal has the same frequency of vibration and its amplitude will be proportional to the magnetic moment, amplitude, and relative position with respect to the pick-up coils system. The sample is fixed to a small sample holder located at the end of a sample rod mounted in an electromechanical transducer. The transducer is driven by a power amplifier which itself is driven by an oscillator at a frequency of 90 Hertz. So, the sample vibrates along the Z axis perpendicular to the magnetizing field.

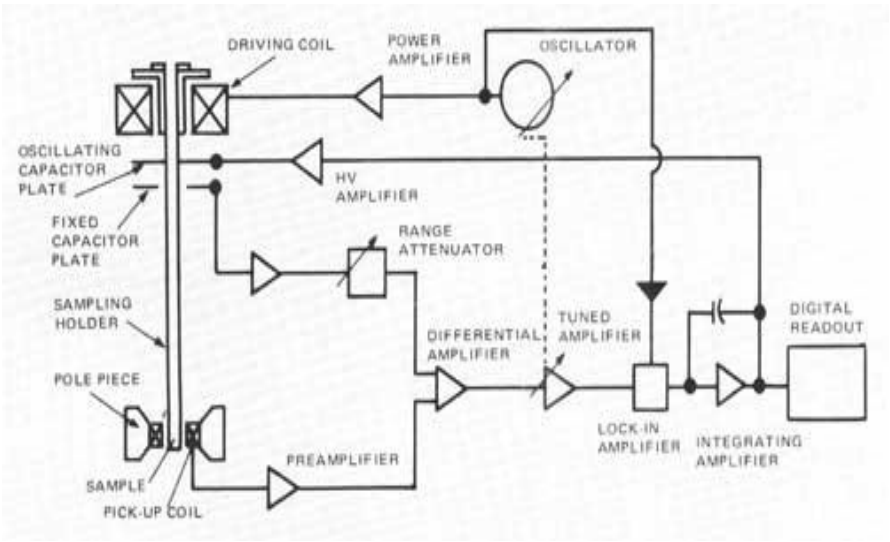


**Figure 3.9:** Schematic of the working principle of VSM

The latter induced a signal in the pick-up coil system that is fed to a differential amplifier. The output of the differential amplifier is subsequently fed into a tuned amplifier and an internal lock-in amplifier that receives a reference signal supplied by the oscillator. The output of this lock-in amplifier, or the output of the magnetometer itself, is a DC signal proportional to the magnetic moment of the sample being studied.

The electromechanical transducer can move along X, Y and Z directions in order to find the saddle point (which Calibration of the vibrating sample magnetometer is done by measuring the signal of a pure Ni standard of known the saturation magnetic moment placed in the saddle point. The basic instrument includes the electromechanical system and the electronic system (including a personal computer), while the costumer should select the electromagnet or superconducting coil system with the appropriate bipolar power supply. Laboratory electromagnets or superconducting coils of various maximum field strengths may be used. For ultra-high magnetic fields a cryogen-free magnets can be also used. For the characterization of soft magnetic materials a pair of Helmholtz coils may be also used.

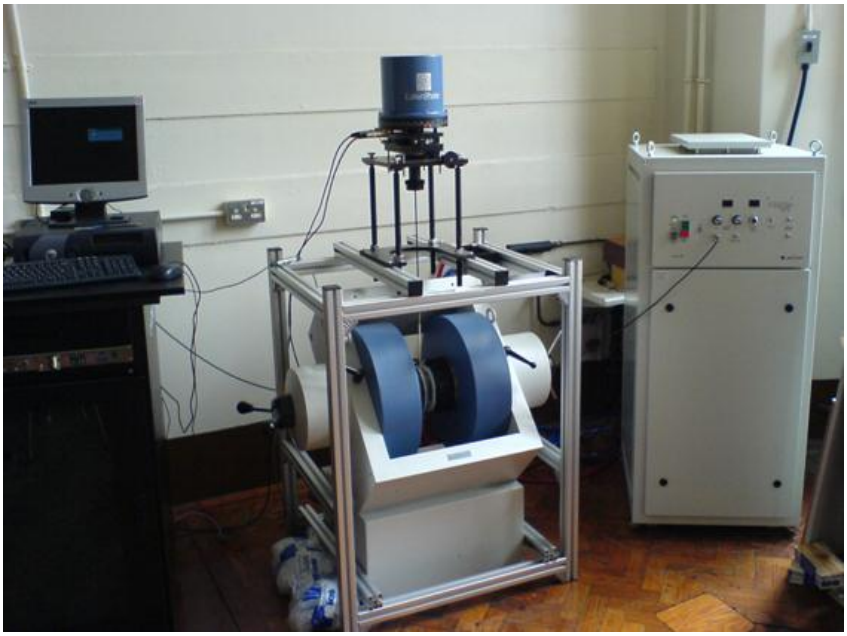

**Figure 3.10:** VSM Set-Up

**Applications**: With the help of vibrating sample magnetometer one can measure the DC magnetic moment as a function of temperature, magnetic field, angle and time. So, it helps in susceptibility and magnetization studies. The most common measurements done are: hysteresis loops, susceptibility or saturation magnetization as a function of temperature (thermo magnetic analysis), magnetization curves as a function of angle (anisotropy) and magnetization as a function of time.

## 4.1 **Structural and phase analysis**

Structural and phase investigation of magnetite nanoparticles and silica coated magnetite nanoparticles has been carried out by powder X-ray diffraction (XRD). X-ray patterns are recorded on PANalytical X'Pert PRO MRD ML. The XRD patterns of the as-synthesized $Fe_3O_4$ nanoparticles and TEOS (silica) –coated $Fe_3O_4$ nanoparticles are shown in figure 1. All the six peaks observed at 2θ ~30.25° (220), 35.75° (311), 43.25° (400), 53.70° (422), 57.45° (511), and 62.70° (440) indexed to a pure cubic inverse spinel structure, indicates the formation of $Fe_3O_4$ phase.

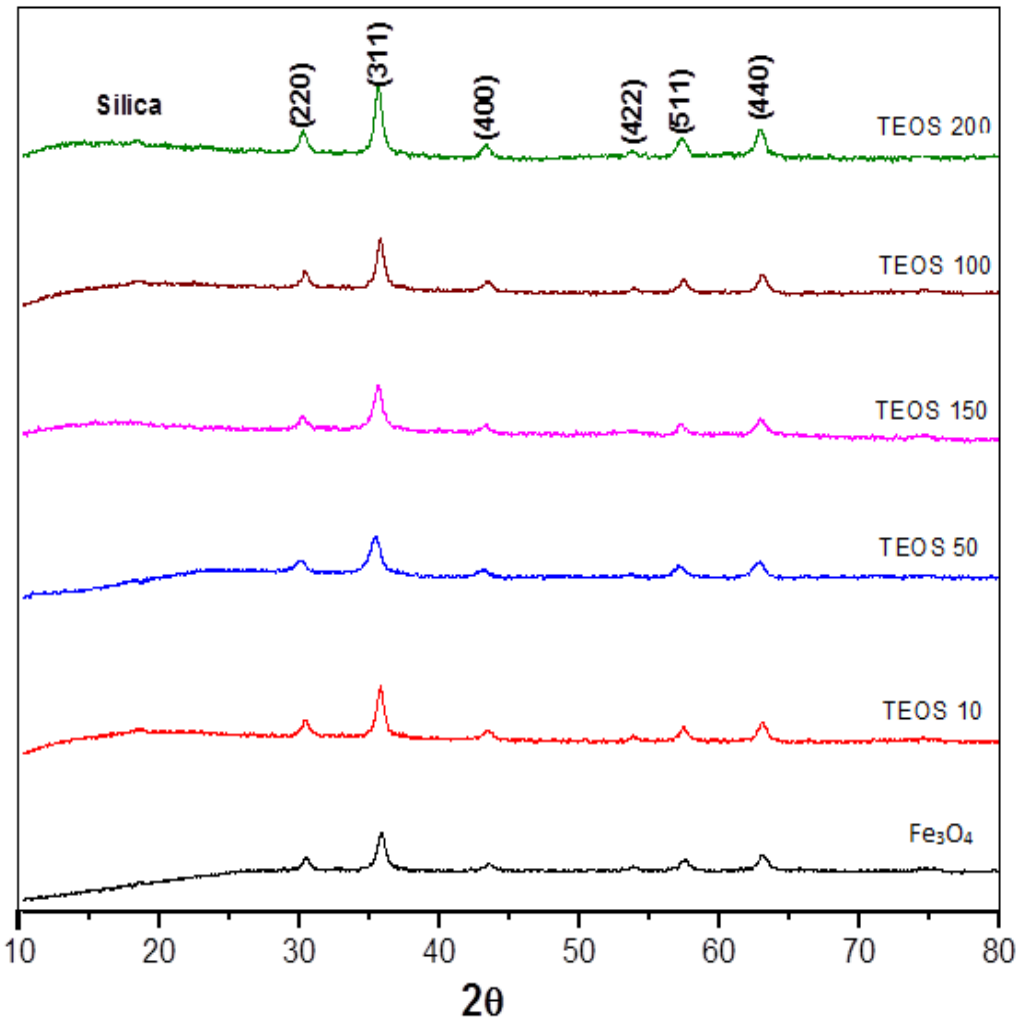


**Figure 4.1** : XRD patterns of uncapped and TEOS capped $Fe_3O_4$ nanoparticles.

All the peaks in the XRD patterns agree well with Joint Committee on Powder Diffraction Standards (JCPDS) reference number 19-0629. The broad hump centered at 23° is due to the presence of amorphous silica [47].

The average crystallites size (D) of uncapped and TEOS capped $Fe_3O_4$ nanoparticles has been calculated using Debye-Scherrer formula [48]

$$D=0.9\,\lambda / \beta \cos\theta$$

where λ is characteristics wavelength used (Cu-Kα = 1.54016 Å), β is the full width at half maxima (FWHM) of highest intense peak (311), and θ is Bragg's angle calculated values are presented in table 2.

**Table 2 Crystallite size calculated from x-ray diffraction**

| S.No | Sample specification | Crystallite size (nm) |
|---|---|---|
| 1. | $Fe_3O_4$ | 13.20 |
| 2. | TEOS 10 | 14.10 |
| 3. | TEOS 50 | 10.05 |
| 4. | TEOS 100 | 15.47 |
| 5. | TEOS 150 | 11.72 |
| 6. | TEOS 200 | 14.00 |

### 4.2 FTIR study

FTIR spectroscopy is an appropriate technique to understand adsorption of polymers/organic or inorganic components on the surface of nanoparticles. FTIR spectra were recorded on a Perkin Elmer Spectrum BX(II) spectrophotometer in the transmission mode with spectroscopic grade KBr pellets for all the powders samples as shown in figure 2. The characteristic absorption bands at 443, 580 and 620 $cm^{-1}$ in the FTIR spectra of magnetite are attributed to asymmetric stretching vibrations of Fe-O. Bands at 580 and 620 $cm^{-1}$ are due to the splitting of the absorption band observed

at 570 $cm^{-1}$ in the spectrum of bulk magnetite. Similarly, the band at 440 $cm^{-1}$ originates from another absorption band of Fe-O of bulk magnetite located at 375 $cm^{-1}$.

The sharp band at 1088 $cm^{-1}$ is corresponding to Si–O–Si anti-symmetric stretching vibrations, being indicative of the existence of $SiO_2$ in the nanostructures. The Si–O–Si bond's asymmetric stretching vibration at 1088 $cm^{-1}$ and symmetric stretching vibration at 800 $cm^{-1}$ appear in all the samples but, which indicates that the silica has successfully coated on the surface of $Fe_3O_4$ nanocrystals by hydrolysis and condensation of TEOS. The absorption bands at about 3427 and 1637 $cm^{-1}$ in all the spectra mainly originate from the–OH vibrations in $H_2O$. Peaks at 2851 and 2915 $cm^{-1}$ is due to $-CH_2$ (stretching vibrations).

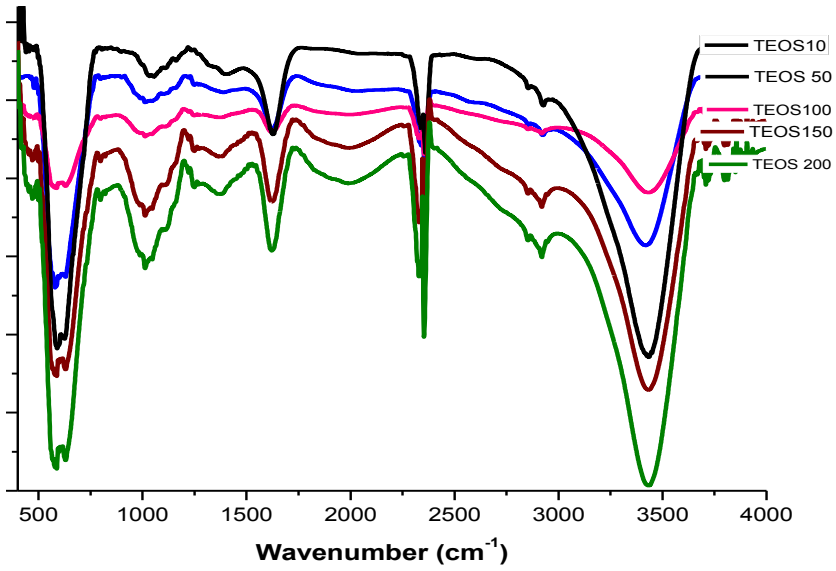


**Figure 4.2**: FTIR spectra of $Fe_3O_4$ nanoparticles coated with different concentrations of TEOS

### 4.3 UV-Visible Spectra

The encapsulation of methylene blue (MB) in magnetite-silica nanoparticles is confirmed by UV-Visible spectroscopy. For UV-Visible study a small sample is disperse in water and this solution is used for the analysis. UV-Visible spectra are recorded on Analticjena Specord 205. Figure 4.3 shows the UV-Visible spectrum of MB loaded magnetite-silica nanoparticles and a broad hump at 657 nm is observed, which corresponds to the characteristic absorption of MB molecule in water.

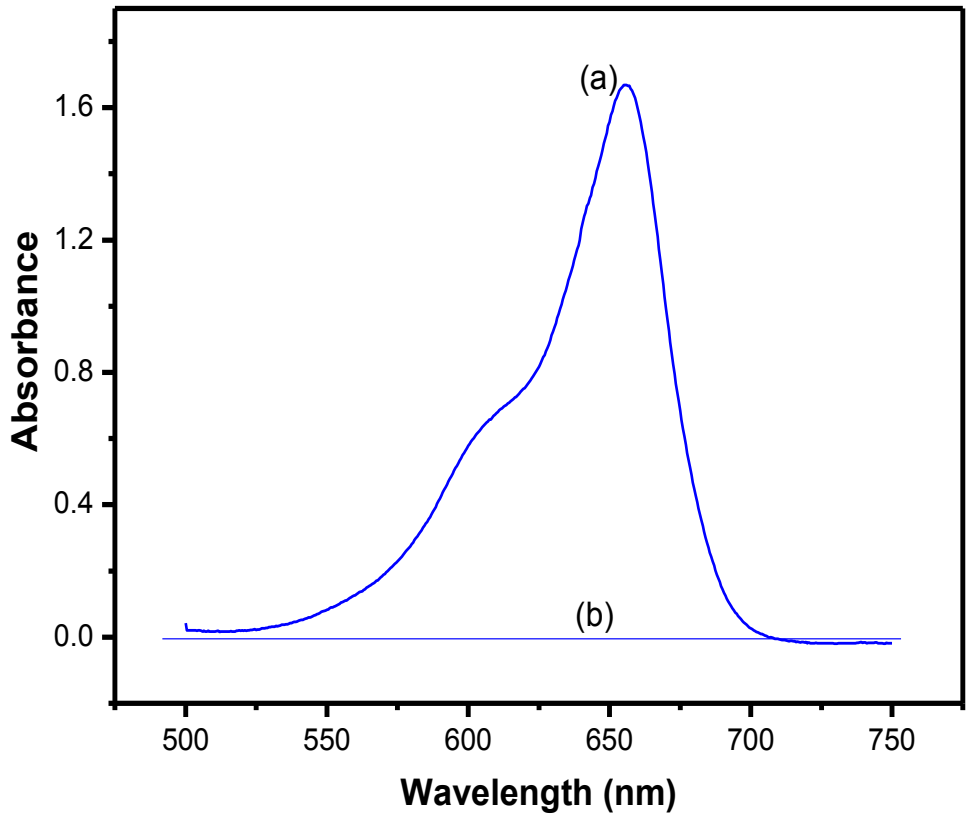


**Figure 4.3:** UV-Visible spectrum of (a) MB loaded magnetite-silica nanoparticles and (b) magnetite-silica nanoparticles.

### 4.4 Morphological study

#### 4.4.1 TEM analysis

The morphological study of magnetite nanoparticles has been done by TEM. TEM micrograph has been recorded on JEOL (GEM 200) high resolution electron microscope. For TEM analysis a small sample is disperse in ethanol and the drop of this solution taken on carbon coated copper grid. Figure 4 shows the TEM micrographs of $Fe_3O_4$ nanoparticles. It is clear from the figure 4.4 that the nanoparticles are polydisperse with nearly spherical morphology.The size distribution histogram of nanoparticles is also shown as inset in figure. The average size of the nanoparticles is 14.39 nm $\pm$ 1.66 nm with a polydispersity index of 0.12 % [49].

#### 4.4.2 SEM analysis

To study morphology of synthesised magnetite nanoparticles coated with different concentrations of TEOS by SEM. For SEM analysis, the dried sample of synthesized nanoparticles was coated with gold-palladium alloy using JEOL, JFC sputter coater

and then examined under JEOL, JSM-6510 L scanning electron microscope. Figure 5 shows SEM microscope of synthesized nanoparticles. It is clear from the figure 5 that the particles are non-uniform in size and shape. No characteristic morphology is observed in any sample. This might be due to agglomeration of nanostructures.

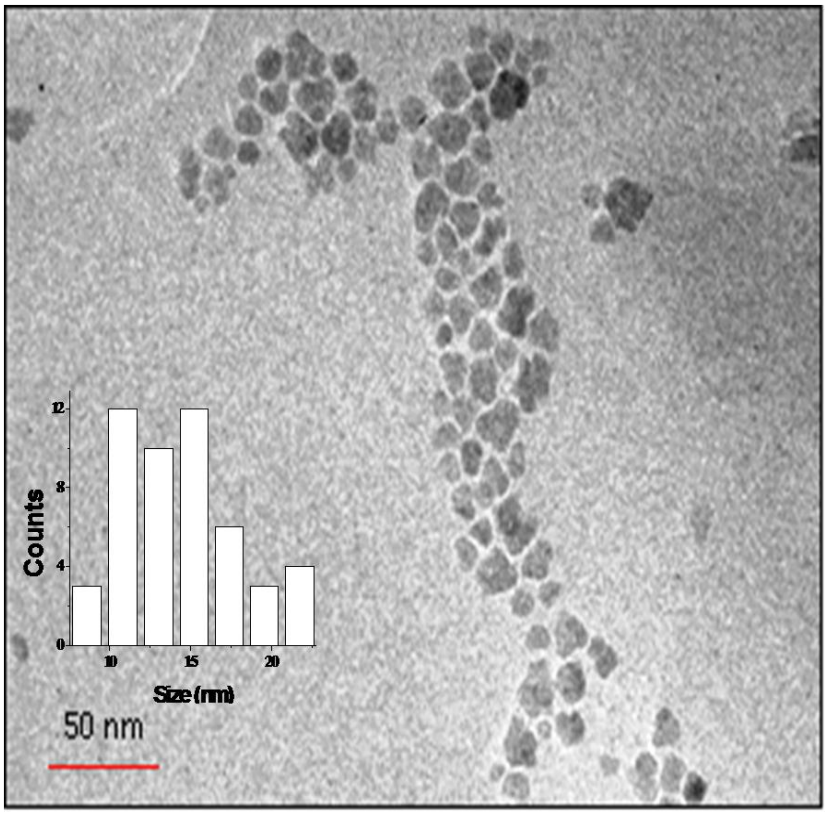


**Figure 4.4**: TEM micrographs of $Fe_3O_4$ nanoparticles

### 4.5 Magnetic Study

The magnetic study of synthesized nanoparticles has been performed using VSM. It is clear from figure 4.6 that as the applied magnetic field increases the magnetization increases and also, the saturation achieved at the higher field. These nanoparticles are superparamagnetic in nature so that's why this type of saturation is observed. Silica is diamagnetic in nature, therefore so the magnetization reduces as the capping concentration of TEOS increases.

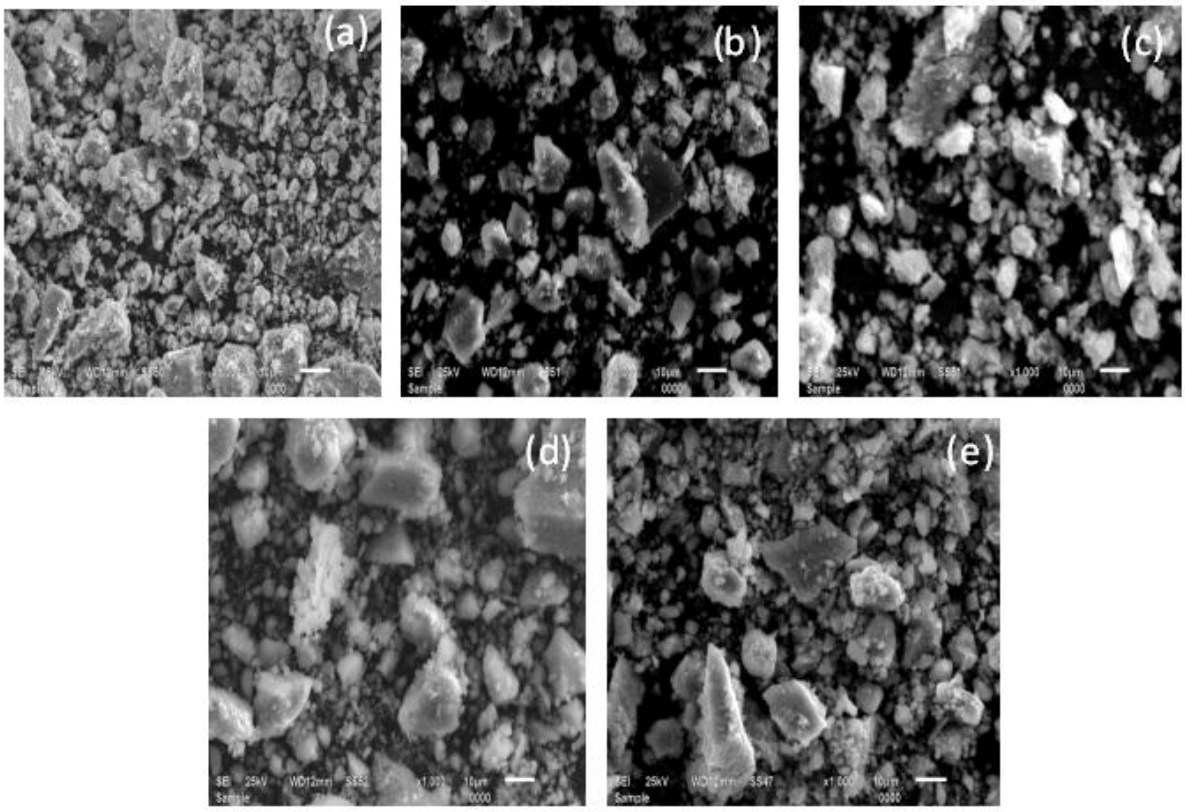


**Figure 4.5:** SEM micrograph of $Fe_3O_4$-$SiO_2$ core-shell nanostructures with different concentrations of TEOS (a) 10 µL (b) 50 µL (c) 100 µL (d) 150 µL and (e) 200 µL.

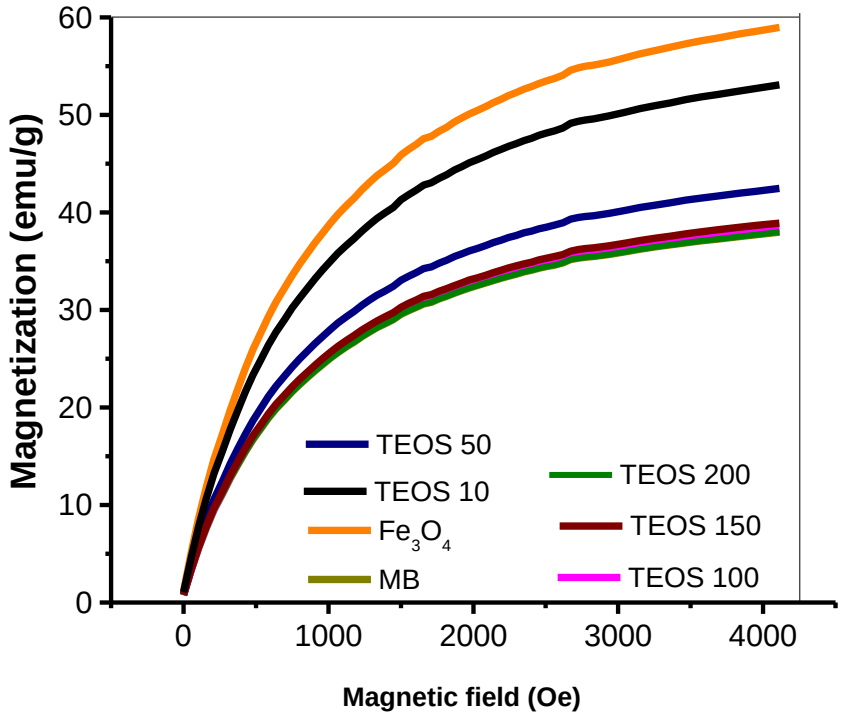


**Figure 4.6:** Magnetization curve of Magnetite and silica coated magnetite core-shell nanostructures

**Table 3:** Magnetization value of $Fe_3O_4$ and TEOS capped nanoparticles.

| S. No. | Sample code | Magnetization (emu/g) |
|---|---|---|
| 1. | $Fe_3O_4$ | 58.97 |
| 2. | TEOS 10 µL | 53.07 |
| 3. | TEOS 50 µL | 42.45 |
| 4. | TEOS 100 µL | 38.33 |
| 5. | TEOS 150 µL | 38.20 |
| 6. | TEOS 200 µL | 37.97 |
| 7. | MB | 37.97 |

## 4.6 Conclusions

- Magnetite nanoparticles have been prepared by chemical co-precipitation method.
- Inorganic silica coating of variable thickness has been achieved on the surface of magnetite nanoparticles by hydrolysis and condensation of tetraethyl orthosilicate (TEOS).
- XRD study confirms the cubic inverse spinel structure of $Fe_3O_4$ nanoparticles. The average crystallite size of the magnetite nanoparticles obtained from the peak broadening was 13 nm.
- FTIR study also confirms the bonding of silica on the surface of magnetite nanoparticles.
- UV-Visible spectrum of methylene blue loaded magnetite-silica nanoparticles shows a broad hump at 657 nm is observed, which confirms the loading of methylene blue in the silica matrix.
- TEM study reveals that the nanoparticles are polydisperse with nearly spherical morphology. The average size of the nanoparticles is 14.39 nm $\pm$ 1.66 nm with a polydispersity index of 0.12 %.

- SEM study shows that the core-shell particles are non-uniform in size and shape. No characteristic morphology is observed in any sample. This might be due to agglomeration of nanostructures.
- The magnetic measurements confirms that as-synthesized and silica coated magnetite nanoparticles are superparamagnetic in nature with a fairly high saturation magnetisation. The Ms value decreases as the coating thickness of silica increases in the samples. This is attributed to increasing diamagnetic contribution from the shell.
- These core-shell nanostructures can be used for imaging and therapy purposes. The presence of methylene blue in magnetite-silica core-shell nanostructure will likely to enhance the contrast in the MRI imaging. Further, they can also be used to treat malignant tumours by means of photodynamic therapy.

## References


[1] K K Jain, Technology in Cancer Research and Treatment 4 (2005) 1533.

[2] J K Vasir, M S V Labhasetwar, Technology in Cancer Research and Treatment, 4 (2005) 363.

[3] Tomalia D.A.,Prog.Polym,Sci 30 (2005)294

[4] Jurgons R, Magn.Reson.Med 53 (2005) 999

[5] Ferrari M, Nat.Rev.Cancer 5 (2005)161

[6] Bigger I, Adv.Drug Delivery Rev. 54 (2002) 631

[7] Bogdanov A, J Drug Targeting 4 (1997) 321

[8] Cancer Reference Information, American Cancer Society,Inc (2006)

[9] Hobbs,S.K,et al,Proc.Natl.Acad.Sci.,USA 95 (1998) 4607

[10] Okuhata,Y,,Adv.Drug Delivery Rev. 37 (1999)121

[11] Au J L, Jang S H,Wientjes M G, J Control Release 78 (2002) 81

[12] Bogdanov,A J Drug Targeting 4(1997) 321

[13] BenjaminL,"Implementation of a spatially-resolved explicit photodynamic therapy dosimetry system utilizing multi-sensor fiber optic probes", M.Sc. Thesis, University of Toronto , 2009, 112 pages; MR59238

[14] M arrebo, R F Pacheco, M R Ibarra, J Santamaria, Nanotoday, 2, 2007, 22

[15] M. Babincova, P. Babinec ,Biomed Pap Med Facunivpalacky Olomouc Czech Repub. 153 (2009) 243.

[16] Raab O., Z. Biol, 39 (1990) 524

[17] Plicard A.Etudes, Compt.Rend.Soc.Biol, 91 (1924) 1423

[18] Ronchese F., Oral.Med.Oral.Path., 7 (1954) 967

[19] Figge FHJ., Research Conf. On Cancer. Moulton, (1945) 117

[20] Rasmussen-Taxdal DS, Ward DE, Figge FHJ., Cancer, 8 (1955) 78

[21] Winkelman J., J.Natl. Cancer Inst., 27, (1961) 1369

[22] Lipson RL, Baldes EJ, Olsen AM, J. Natl. Cancer Inst. 26 (1961) 1

[23] Henderson BW, Dougherty TJ, Schwartz S, Photodynamic Theraphy: Basic Principles and Clinical Applications, 1992

[24] Dougherty TJ, J. Clin. Laser Med. Surg. 14 (1996) 219

[25] BenjaminL,"Implementation of a spatially-resolved explicit photodynamic therapy dosimetry system utilizing multi-sensor fiber optic probes", M.Sc. Thesis, University of Toronto , 2009, 112 pages; MR59238

[26] Dolmans D, Fukumura D, Rakesh K. Jain, Nature Reviews Cancer, 3 (2003) 380

[27] Y P He, S Q Wang, C R Li, Y M Miao, Z Y Wu, B S Zou, J. Phys. D: Appl. Phys.38 (2005) 1342.

[28] Xie J, K Chen, H Y Lee, C Xu, A R Hsu, S Peng, X Chen, S Sun, J. Am. Chem. Soc. 130 (2008) 7542.

[29] Tada D B, L L R. Vono, E L Duarte, R Itri, P K Kiyohara, M S Baptista, L M Rossi, Langmuir 23 (2007) 8194.

[30] Barick K C, D Bahadur, Bull. Mater. Sci., 29 (2006) 595.

[31] Chen F H, Q Gao, J Z Ni, Nanotechnology 19 (2008) 165103

[32] Qing C, L Zhu , C Yu, H Tang, J. Luminescence 128 (2008) 1890

[33] S Thomas, D Sakthikumar, P A Joy, Y Yoshida, M R Anantharaman, Nanotechnology 17 (2006) 5565

[34] Y Chujo, H Matsuki, S Kure, T Saegusa, Yazawa T , Chem. Soc. Chem. Comm.5 (1994) 635

[35] C Seup, L Sun, P Bin, O Kikuo J. Chem. Eng. of Jpn. 37 (2004) 1099

[36] S Tsang, C Yu, X Gao, K Tam, J. Phys. Chem. B 110 (2006) 16914

[37] R He, X You, J Shao, F Gao, B Pan, D Cui, Nanotechnology 18 (2007) 315601

[38] Y Deng, C Wang, J Hu, W Yang, S Fu, Colloids and Surfaces A 262 (2005) 87

[39] C Huang, C Hou, C Chen, Y Tsai, L Chang, H Wei, K Hsieh, C Chan Nanotechnology 19 (2008) 55701

[40] R Mehta, R Upadhyay, S Charles, C Ramchand Biotechnology Techniques 11 (1997) 493

[41] W Stobber, A Fink, E Bohn J. Colloid and Interface Sci. 26 (1968) 62

[42] N Andhariya, B Chudasama, R V Mehta, R V Upadhyay, J. Nanoparticle Research 13(2011) 1677

[43] S Chen, P Dong, G Yang, J Yang Ind. Eng. Chem. Res. 35 (1996) 4487

[44] Y He, S Wang, C Li, Y Miao, Z Wu, B Zou J. Phys. D 38 (2005) 1342

[45] S Sapra, J Poppe, A Eychmiiler, Small 3(2007)1886

[46] G Pastorin, Pharma. Res 26 (2008) 74

[47] Y P He, S Q Wang, C R Li, Y M Miao, Z Y Wu, B S Zou, J. Phycs. D: Appl. Phys. 38 (2005) 1342

[48] B D Cullity, Elements of x-ray diffraction, Addison-Wesley Pub. Co., 1978

[49] N Andhariya, B Chudasama, R V Mehta, R V Upadhyay, J. Nanoparticle Research 13 (2011) 1677